Super-resolution Optical Spectroscopy of Nanoscale Emitters within a Photonic Atom Probe

Enrico Di Russo, Pradip Dalapati, Jonathan Houard, Linda Venturi, Ivan Blum, Simona Moldovan, Nolwenn Le Biavan, Denis Lefebvre, Maxime Hugues, Didier Blavette, et al.

Super-resolution Optical Spectroscopy of Nanoscale Emitters within a Photonic Atom Probe

Enrico Di Russo, Pradip Dalapati, Jonathan Houard, Linda Venturi, Ivan Blum, Simona Moldovan, Nolwenn Le Biavan, Denis Lefebvre, Maxime Hugues, Jean Michel Chauveau, Didier Christian Blavette, Bernard Deconihout, Angela Vella, François Vurpillot, and Lorenzo Rigutti*

https://dx.doi.org/10.1021/acs.nanolett.0c03584

ABSTRACT: Atom Probe Tomography (APT) is a microscopy technique allowing for the 3D reconstruction of the chemical composition of a nanoscale needle-shaped sample with a precision close to the atomic scale. The photonic atom probe (PAP) is an evolution of APT featuring in situ and operando detection of the photoluminescence signal. The optical signatures of the light-emitting centers can be correlated with the structural and chemical information obtained by the analysis of the evaporated ions. It becomes thus possible to discriminate and interpret the spectral signatures of different light emitters as close as 20 nm, well beyond the resolution limit set by the exciting laser wavelength. This technique opens up new perspectives for the study of the physics of low dimensional systems, defects and optoelectronic devices.

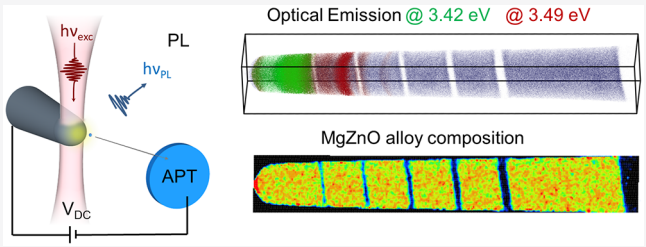

KEYWORDS: *Super-resolution, Optical Spectroscopy, Atomic Scale Microscopy, Semiconductors, Heterostructures, Quantum Light Emitters*

With the development of microscopy techniques with nearly atomic or atomic resolution, the possibility to correlate the optical properties of a nanoscale object and its structural properties yields a key for the understanding of the mechanisms of light−matter interaction and for the optimization of light emitters or absorbers: the size and the composition of a quantum dot, for instance, contribute to the determination of the energy of the emitted photons. An important quantity in these techniques is the spatial resolution of optical spectroscopy, i.e., the distance over which it is possible to identify distinct features in two different spectra. Scanning transmission electron microscopy (STEM) yields atomic scale images and can be associated with cathodoluminescence (CL) for the study of radiative transitions (STEM-CL)[1] or to electron energy loss spectroscopy (EELS) for the study of plasmon excitations.[2] In these cases, the spatial resolution of the optical measurement can be close to several nanometers. A three-dimensional morphological analysis can be achieved in electron microscopy by coupling CL with electron tomography (ET).[3] Sublattice resolution can be achieved by scanning tunneling microscopy (STM) coupled to electroluminescence (EL) spectroscopy.[4] However, this technique is limited to surfaces.

The unique property of atom probe tomography (APT) is the 3D atomic-scale reconstruction of small analyzed volumes ($\sim 50 \times 50 \times 50$ nm^3), allowing for a direct assessment of the local chemical composition.[5−7] As an evolution of laser-assisted-APT[8] in which ion evaporation is controlled by laser pulses, a 3D photonic atom probe (PAP) features in situ and operando PL coupled with APT analysis.[9] During the analysis, the series of collected spectra evolves smoothly due to the slow and controlled evaporation of the atomic monolayers constituting the specimen. It becomes thus possible to discriminate the spectral features of distinct spatial regions lying at distances much lower than the diffraction limit of the exciting laser (i.e., performing super-resolution spectroscopy) and to simultaneously correlate this information with the 3D structure of nanoscale light emitters in terms of chemical composition, interface definition, and morphology.

The schematics of a PAP is reported in Figure 1a.[9] The nanometric needle-shaped specimen is polarized with a voltage V_{DC} = 3−16 kV, leading to an apex electric field of a few tens of volts per nanometer.[8,10] Field ion evaporation is then triggered by femtosecond laser pulses at the cadency of 400 kHz. The evaporated ions are detected by a time-resolved and position sensitive detector,[11] which provides the impact position of ions and their time-of-flight. The first information is used to calculate the position of evaporated atoms at the tip

Received: September 4, 2020
Revised: November 10, 2020

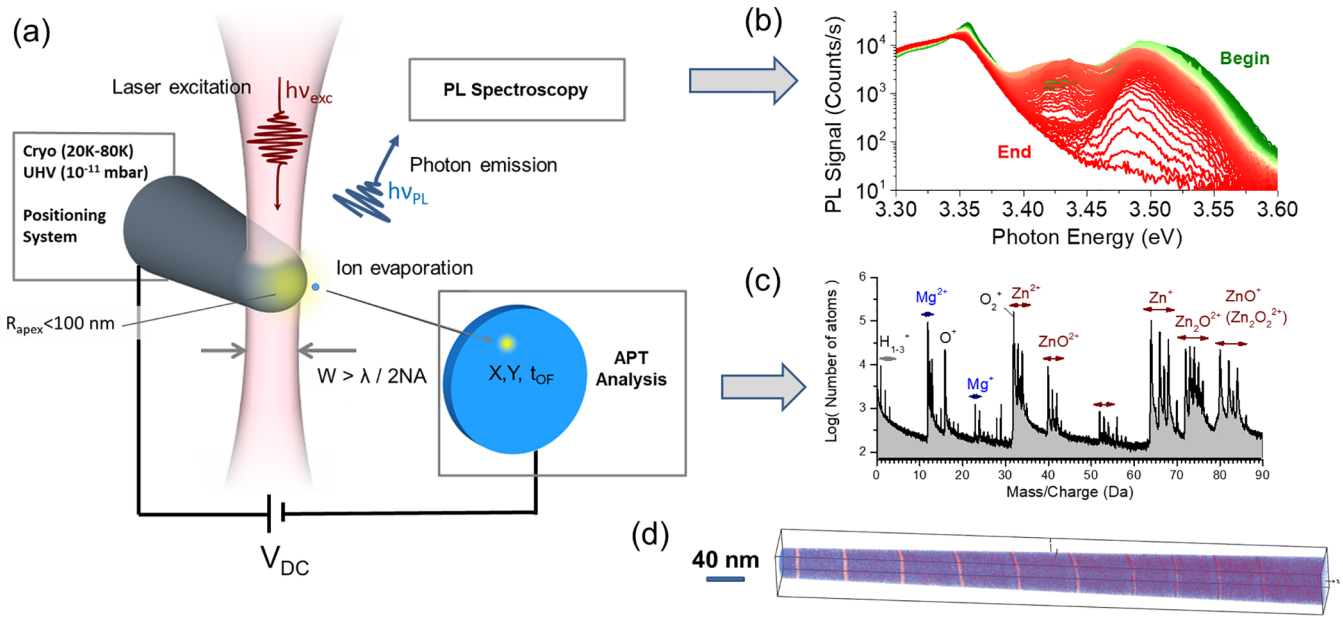

Figure 1. Photoluminescence in situ in a photonic atom probe. (a) Principle of the instrument: pulsed laser focused close to the diffraction limit impinging on a specimen tip immerged in an intense electrostatic field. Laser pulses trigger both ion evaporation and photon emission. The specimen is thus progressively evaporated during the analysis. (b) Analysis of PL results in a series of spectra where the spectral components progressively disappear due to the erosion of the tip. (C, D) Analysis of the ion impacts on the 2D position- and time-of-flight-sensitive detector, allowing for standard APT analysis, where the chemical nature of the ion can be identified in a (c) mass histogram and (d) a 3D reconstruction of the analyzed volume within the field of view of the detector can be calculated.

surface, while the second is used to compute mass/charge ratios that enable one to identify the chemical nature of atoms, as shown in the mass spectrum of Figure 1c. The in-depth layer by layer evaporation of the specimen makes the 3D reconstruction of atomic positions possible. Three-dimensional maps of the chemical composition of the specimen can thus be derived, as shown in Figure 1d. The instrument is able to collect and analyze in situ and in real time the photoluminescence that laser pulses excite simultaneously with surface atom evaporation.[9] The collection of the PL signal during APT translates into a series of spectra such as that reported in Figure 1b. The optical information can then be retrieved from the analysis of single or multiple spectra. In particular, it is possible to analyze differential spectra, i.e., the difference between the signal of two PL spectra $\Delta S(i,i+1) = S(i) - S(i+1)$ with i indexing the acquisition sequence. (See Materials and Methods and the Supporting Information for further details.)

In situ PAP was applied to heterostructures on the basis of ZnO/(Mg,Zn)O multilayers containing semipolar quantum wells (QWs) grown on the wurtzite r-plane.[12] They are considered for the development of devices based on quantum confinement.[13−16] Independent accurate measurement of layer thicknesses, representing a reference scale for the APT reconstruction, was performed by TEM, as detailed in the Supporting Information.

The PAP analysis of a tip is reported in detail in Figure 2. Two PL spectra, S(1) and S(38), are reported in Figure 2a. S(1) was acquired at the beginning of the tip evaporation, so it contains the spectral signature of various emitters within the specimen. Spectrum S(38) was acquired after the evaporation of QW1, the one closest to the ZnO substrate. The peak at 3.35 eV corresponds to the emission of the ZnO substrate, the peak at 3.7 eV to emissions taking place within the (Mg,Zn)O barriers, while all peaks between them, appearing in the S(1) spectrum, are to be ascribed to the five QWs. The complete series of the S(i) spectra and of the differential spectra $\Delta S(i,i+1) = S(i) - S(i+1)$ are reported in Figure 2b,c, respectively. The reconstructed positions of the Mg atoms and the Mg/(Mg+Zn) fraction map calculated on a 5 nm thick slice close to the tip axis are reported in Figure 2d,e, respectively. The position of the specimen surfaces at specific spectrum indices i are reported as dashed red lines. APT data show the position and the morphology of the different QWs, exhibiting nearly planar interfaces; The thickness of the QWs is $t_{QW5} = 0.5 \pm 0.2$ nm, $t_{QW4} = 0.9 \pm 0.2$ nm, $t_{QW3} = 1.8 \pm 0.3$ nm, $t_{QW2} = 3.2 \pm 0.3$ nm, and $t_{QW1} = 4.0 \pm 0.3$ nm. Statistical first nearest-neighbor analysis[17] also indicates a nearly random Mg distribution, with average Mg/(Mg+Zn) fraction $y = 0.14 \pm 0.01$. It is also apparent that QW interface fluctuations can occur, spanning one or several monolayers. The series of PL spectra in Figure 2b shows, from top to bottom, the progressive bleaching of the spectral components relative to the (Mg,Zn)O barrier and to the QWs. The differential PL spectra of Figure 2c highlight the variations in consecutive spectra, which are largest when the emitter related to the spectral component is close to evaporation. The blue circles highlight the position of the signatures of QWs 5 to 2, appearing as red spots in the plot. The differential PL signals at 3.49 and 3.42 eV are color-coded into the Mg atom distribution of Figure 2d. The spatial regions corresponding to the emission of QW5 and QW4 appear as clearly distinguished. It becomes then possible to attribute an average emission energy to each QW, with the exception of QW1. The interwell distance is as low as 22 nm. It can be expected that the discrimination of two emitters at even closer distances could be achieved, provided the spectral signatures do not significantly overlap. The signal of QW1 overlaps with the ZnO signal, which is in turn affected by amplitude oscillations whose origin is currently under study.

https://dx.doi.org/10.1021/acs.nanolett.0c03584

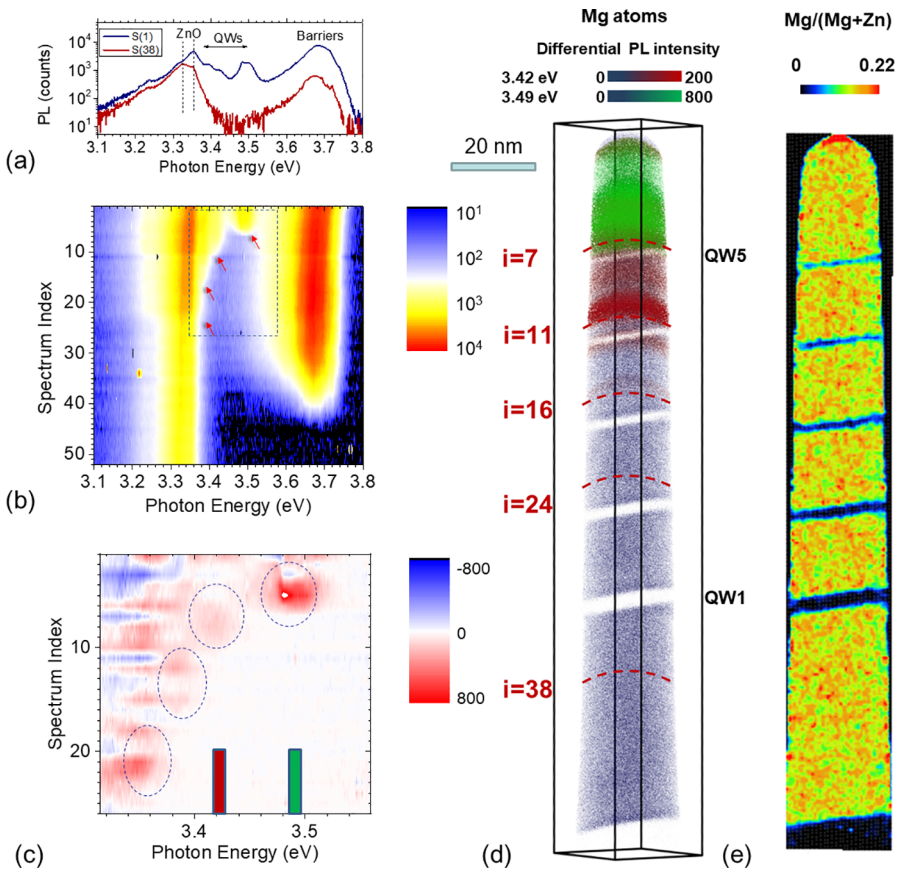

Figure 2. In situ μPL-APT analysis. (a) PL spectra collected at the beginning of the evaporation process (S(1)) and shortly after the evaporation of the last quantum well (S(38)). The spectral contributions can be grouped into emissions originated by the ZnO substrate, by the QWs and by the (Mg,Zn)O barriers. (b) Complete set of collected μPL spectra, the red arrows indicating the approximate location of the disappearance of the PL peaks of consecutive QWs. (c) Differential spectra within the region indicated by the dashed rectangle in panel b. The optical signatures of 4 over 5 quantum wells are highlighted by the blue circles, while the colored rectangle corresponds to the spectral intervals selected for the color coding of the Mg atom positions in panel d. (d) 3D reconstruction of the positions of Mg atoms and (e) 2D distribution of the Mg II-site fraction calculated over a 5 nm thick slice close to the tip axis. The red dashed lines indicate the approximate position of the specimen surface during the acquisition of the *i*th spectrum, while the color coding of the Mg atoms indicates the intensity of the differential PL signal around 3.49 eV (green, originating from QW5) and 3.42 eV (red, QW4). Animated graphics are available in the Supporting Information (Movies S1 and Movie S2).

As the specimen is in-depth analyzed (S(1) to S(38), Figure 2a) and approaching the substrate, both a red shift of the asymmetric barrier peak related to MgZnO barrier (E = 3.683 eV at the beginning of evaporation and E = 3.67 at the end) and a low-energy broadening within the ZnO peak can be observed. As the APT reconstruction indicates a uniform average composition throughout all barriers, these red shifts are ascribed to the progressive increase of the stress induced by the DC electric field on the tip apex.[18] In perspective, these strain-related phenomena open the way to the study of stress states, elastic constants, and deformation potentials.

The reproducibility of these results is confirmed by the analysis of a different sample, grown on the nonpolar m-plane, reported in the Supporting Information.

The bridge between PL spectra and APT reconstruction is based on the solution of the strain, Poisson and effective mass Schrödinger equations.[19] The method is applied on the basis of the results of past works on heterostructures, in which it was possible to correlate the optical signatures and the 3D microscopic structure of quantum confined emitters.[20,21] An important observation is that interfaces can be affected by thickness fluctuations of one monolayer width and several nanometer lateral extension, as it can be inferred from APT 3D reconstructions. The effective mass calculations yield two main results: interface fluctuations can lead to localization of both electrons and holes. The localization is higher for holes due to their higher effective mass. Furthermore, as shown in Figure 3, the emission energies calculated as a function of the QW thickness measured by PAP are in reasonable agreement with the experimental values extracted directly from PL data. No fitting parameters or procedures were adopted. The dynamic spectral shifts observed during evaporation are not considered in the model. Although the phenomenon is not as visible in the case of QWs as in the case of the barrier, these shifts may be of the order of 10−20 meV, which is lower than the full width at half-maximum of the QW peaks. Also not considered in the model was the possibility of surface band bending, because this phenomenon is predicted to be negligible due to strong free charge accumulation at the apex surface.[22]

It should be underlined that the transition energies calculated without assuming interface fluctuations were not significantly different in energy (some millielectronvolts only), a quantity that is lower than the uncertainties affecting the exciton binding energy. Furthermore, QW transitions tend to cross the ZnO near band edge (NBE) emission for large QW thickness, which is a manifestation of the quantum confined

https://dx.doi.org/10.1021/acs.nanolett.0c03584

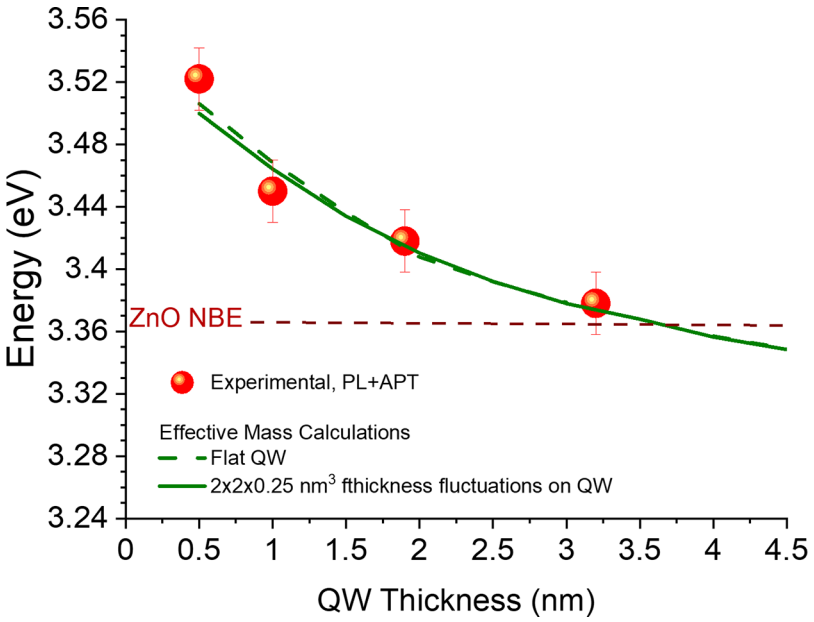

Figure 3. Correlation of the optical and structural properties of quantum wells. The experimental PL energies are plotted versus the QW thickness measured by APT (red dots) for the r-plane sample. Comparison is made with the effective mass calculations performed using two different assumptions (green solid and dashed lines). The red dashed line indicates the energy of the ZnO near band edge (NBE) emission. Error bars correspond to the full width at half-maximum of the differential PL peak.

Stark effect (QCSE) due to the internal electric field setting up across the semipolar ZnO/(Mg,Zn)O interfaces.

In summary, super-resolution PL can be achieved within a photonic atom probe, where optical spectroscopy is performed during the evaporation of the sample. The optical information can be correlated to the structural/chemical information obtained by APT analysis. In perspective, this technique can be applied on a large variety of nanoscale systems. The approach can be generalized to emissions from quantum dots, semiconductor alloys, binary compounds, and even to point and extended defects exhibiting optical emission properties.

MATERIALS AND METHODS

A. Photonic Atom Probe. A photonic atom probe is a tomographic atom probe coupled with a microphotoluminescence (μPL) bench, as reported in Figure 1a and technically detailed in ref 9. The nanometric needle-shaped specimen is polarized with a voltage V_{DC} = 3−16 kV, leading to an apex electric field of a few tens of volts per nanometer.[8,10] Field ion evaporation is then triggered by femtosecond laser pulses at the cadency of 400 kHz. The specimen apex is illuminated by a laser spot with size close to 1 μm. This size is limited by the imperfections of optical elements and is larger than the diffraction limit $w \approx \lambda/(2\mathrm{NA})$ = 443 nm, where λ = 266 nm is the laser wavelength and NA = 0.3 is the numerical aperture of the focusing optics. PL spectra were acquired with a 600/mm grating in a 320 mm focal length spectrometer, with a spectral resolution of around 0.1 nm. The CCD array integration time for each acquisition was set to 180 s.

The collection of the PL signal during APT translates into a series of spectra which are indexed by the integer i while keeping track of the progressive number of detected atoms

B. Details on Sample Growth and Specimen Preparation. Plasma assisted molecular beam epitaxy (PA-MBE) was used to grow the ZnO/(Zn,Mg)O homoepitaxial MQWs on r-plane (10−12) or m-plane (10−10) ZnO substrates. Details on the homoepitaxial growth can be found in ref 23. The structures contain an alternance of ZnO QWs and (Mg,Zn)O barriers. The total thickness and the alloy composition of the multiple layer structure was designed in order to avoid plastic relaxation.

Lamella and field emission tip specimens were prepared by focused ion beam (FIB) in a ZEISS Nvision 40 dual beam SEM-FIB system. The preparation consisted of the standard protocol of lift-out and milling using an acceleration voltage of 30 kV for the Ga ions during sample milling, with a final cleaning step at 2 kV.[24]

C. Calculation of Electronic States. Calculations of electronic wave functions were performed by solving the Schrödinger and Poisson equations in a self-consisted manner, using the **k·p** effective mass model within the framework of the Nextnano software.[19] Details about the calculations are given in the Supporting Information.

ASSOCIATED CONTENT

Supporting Information

The Supporting Information is available free of charge at https://pubs.acs.org/doi/10.1021/acs.nanolett.0c03584.

Details about the definition of differential spectra, supporting electron microscopy, complementary PAP analyses, and effective mass calculations (PDF)

Movie S1 containing animated graphic of the PAP analysis illustrated in Figure 2 (AVI)

Movie S2 containing animated graphic of the PAP analysis illustrated in Figure S5 (AVI)

AUTHOR INFORMATION

Corresponding Author

Lorenzo Rigutti − *UNIROUEN, CNRS, Groupe de Physique des Matériaux, Normandie Université, 76000 Rouen, France;* orcid.org/0000-0001-9141-7706;
Email: lorenzo.rigutti@univ-rouen.fr

https://dx.doi.org/10.1021/acs.nanolett.0c03584

Authors

Enrico Di Russo − *UNIROUEN, CNRS, Groupe de Physique des Matériaux, Normandie Université, 76000 Rouen, France*
Pradip Dalapati − *UNIROUEN, CNRS, Groupe de Physique des Matériaux, Normandie Université, 76000 Rouen, France*
Jonathan Houard − *UNIROUEN, CNRS, Groupe de Physique des Matériaux, Normandie Université, 76000 Rouen, France*
Linda Venturi − *UNIROUEN, CNRS, Groupe de Physique des Matériaux, Normandie Université, 76000 Rouen, France*
Ivan Blum − *UNIROUEN, CNRS, Groupe de Physique des Matériaux, Normandie Université, 76000 Rouen, France;* orcid.org/0000-0002-4729-6510
Simona Moldovan − *UNIROUEN, CNRS, Groupe de Physique des Matériaux, Normandie Université, 76000 Rouen, France*
Nolwenn Le Biavan − *Université Côte d'Azur, CNRS, CRHEA, 06 905 Sophia Antipolis CEDEX, France*
Denis Lefebvre − *Université Côte d'Azur, CNRS, CRHEA, 06 905 Sophia Antipolis CEDEX, France*
Maxime Hugues − *Université Côte d'Azur, CNRS, CRHEA, 06 905 Sophia Antipolis CEDEX, France*
Jean Michel Chauveau − *Université Côte d'Azur, CNRS, CRHEA, 06 905 Sophia Antipolis CEDEX, France*
Didier Christian Blavette − *UNIROUEN, CNRS, Groupe de Physique des Matériaux, Normandie Université, 76000 Rouen, France*
Bernard Deconihout − *UNIROUEN, CNRS, Groupe de Physique des Matériaux, Normandie Université, 76000 Rouen, France*
Angela Vella − *UNIROUEN, CNRS, Groupe de Physique des Matériaux, Normandie Université, 76000 Rouen, France*
François Vurpillot − *UNIROUEN, CNRS, Groupe de Physique des Matériaux, Normandie Université, 76000 Rouen, France*

Complete contact information is available at: https://pubs.acs.org/10.1021/acs.nanolett.0c03584

Author Contributions

E.D.R. contributed to the instrumental development, performed PAP analysis and effective mass simulations, and contributed to manuscript writing; P.D. and L.V. performed PAP analysis; J.H. supervised and performed instrumental development; I.B. performed sample preparation; S.M. performed electron microscopy analysis; N.L.B., D.L., and M.H. performed the MBE growth of the analyzed structures, coordinated and supervised by J.M.C.; B.D., A.V., F.V., and D.C.B. participated to the conception of the PAP technique and in the data analysis; L.R. coordinated the work, performed data analysis, and wrote the manuscript. All authors contributed by critically reading the manuscript.

Funding

This work was funded by the French National Research Agency (ANR) in the framework of the projects EMC3 Labex AQURATE, EMC3 Labex IDEPOP, and ANR-13-JS10-0001-01 TAPOTER, and ANR-11-EQPX-0020 GENESIS and cofunded in the framework of RIN IFROST, EMC3 Labex IDEPOP, and CPER BRIDGE projects by the European Union with European Regional Development Fund (ERDF) and by Region Normandie. The authors from CRHEA also acknowledge funding from the European Union's Horizon 2020 Research and Innovation Program under Grant Agreement No. 665107 (project ZOTERAC).

Notes

The authors declare no competing financial interest.

REFERENCES

(1) Zagonel, L. F.; Mazzucco, S.; Tencé, M.; March, K.; Bernard, R.; Laslier, B.; Jacopin, G.; Tchernycheva, M.; Rigutti, L.; Julien, F. H.; Songmuang, R.; Kociak, M. Nanometer Scale Spectral Imaging of Quantum Emitters in Nanowires and Its Correlation to Their Atomically Resolved Structure. *Nano Lett.* **2011**, *11* (2), 568−573.
(2) Nelayah, J.; Kociak, M.; Stéphan, O.; García de Abajo, F. J.; Tencé, M.; Henrard, L.; Taverna, D.; Pastoriza-Santos, I.; Liz-Marzán, L. M.; Colliex, C. Mapping Surface Plasmons on a Single Metallic Nanoparticle. *Nat. Phys.* **2007**, *3* (5), 348−353.
(3) Atre, A. C.; Brenny, B. J. M.; Coenen, T.; García-Etxarri, A.; Polman, A.; Dionne, J. A. Nanoscale Optical Tomography with Cathodoluminescence Spectroscopy. *Nat. Nanotechnol.* **2015**, *10* (5), 429−436.
(4) Doppagne, B.; Chong, M. C.; Lorchat, E.; Berciaud, S.; Romeo, M.; Bulou, H.; Boeglin, A.; Scheurer, F.; Schull, G. Vibronic Spectroscopy with Submolecular Resolution from STM-Induced Electroluminescence. *Phys. Rev. Lett.* **2017**, *118* (12), 127401.
(5) Blavette, D.; Cadel, E.; Fraczkiewicz, A.; Menand, A. Three-Dimensional Atomic-Scale Imaging of Impurity Segregation to Line Defects. *Science* **1999**, *286* (5448), 2317−2319.
(6) Thompson, K.; Flaitz, P. L.; Ronsheim, P.; Larson, D. J.; Kelly, T. F. Imaging of Arsenic Cottrell Atmospheres Around Silicon Defects by Three-Dimensional Atom Probe Tomography. *Science* **2007**, *317* (5843), 1370−1374.
(7) White, L. F.; Darling, J. R.; Moser, D. E.; Reinhard, D. A.; Prosa, T. J.; Bullen, D.; Olson, D.; Larson, D. J.; Lawrence, D.; Martin, I. Atomic-Scale Age Resolution of Planetary Events. *Nat. Commun.* **2017**, *8* (1), 15597.
(8) Gault, B.; Vurpillot, F.; Vella, A.; Gilbert, M.; Menand, A.; Blavette, D.; Deconihout, B. Design of a Femtosecond Laser Assisted Tomographic Atom Probe. *Rev. Sci. Instrum.* **2006**, *77* (4), 043705.
(9) Houard, J.; Normand, A.; Di Russo, E.; Bacchi, C.; Dalapati, P.; Beainy, G.; Moldovan, S.; Da Costa, G.; Delaroche, F.; Vaudolon, C.; Chauveau, J. M.; Hugues, M.; Blavette, D.; Deconihout, B.; Vella, A.; Vurpillot, F.; Rigutti, L. A Photonic Atom Probe Coupling 3D Atomic Scale Analysis with in Situ Photoluminescence Spectroscopy. *Rev. Sci. Instrum.* **2020**, *91* (8), 083704.
(10) Blavette, D.; Bostel, A.; Sarrau, J. M.; Deconihout, B.; Menand, A. An Atom Probe for Three-Dimensional Tomography. *Nature* **1993**, *363* (6428), 432−435.
(11) Costa, G. D.; Wang, H.; Duguay, S.; Bostel, A.; Blavette, D.; Deconihout, B. Advance in Multi-Hit Detection and Quantization in Atom Probe Tomography. *Rev. Sci. Instrum.* **2012**, *83*, 123709−123709.
(12) Chauveau, J.-M.; Teisseire, M.; Kim-Chauveau, H.; Deparis, C.; Morhain, C.; Vinter, B. Benefits of Homoepitaxy on the Properties of Nonpolar (Zn,Mg)O/ZnO Quantum Wells on a-Plane ZnO Substrates. *Appl. Phys. Lett.* **2010**, *97* (8), 081903.
(13) Le Biavan, N.; Hugues, M.; Montes Bajo, M.; Tamayo-Arriola, J.; Jollivet, A.; Lefebvre, D.; Cordier, Y.; Vinter, B.; Julien, F.-H.; Hierro, A.; Chauveau, J.-M. Homoepitaxy of Non-Polar ZnO/(Zn,Mg)O Multi-Quantum Wells: From a Precise Growth Control to the Observation of Intersubband Transitions. *Appl. Phys. Lett.* **2017**, *111* (23), 231903.
(14) Montes Bajo, M.; Tamayo-Arriola, J.; Hugues, M.; Ulloa, J. M.; Le Biavan, N.; Peretti, R.; Julien, F. H.; Faist, J.; Chauveau, J.-M.; Hierro, A. Multisubband Plasmons in Doped $\mathrm{Zn}\mathrm{O}$ Quantum Wells. *Phys. Rev. Appl.* **2018**, *10* (2), 024005.
(15) Tokura, Y.; Kawasaki, M.; Nagaosa, N. Emergent Functions of Quantum Materials. *Nat. Phys.* **2017**, *13* (11), 1056−1068.

https://dx.doi.org/10.1021/acs.nanolett.0c03584

(16) Kang, J.-W.; Song, B.; Liu, W.; Park, S.-J.; Agarwal, R.; Cho, C.-H. Room Temperature Polariton Lasing in Quantum Heterostructure Nanocavities. *Sci. Adv.* **2019**, *5* (4), No. eaau9338.
(17) Philippe, T.; De Geuser, F.; Duguay, S.; Lefebvre, W.; Cojocaru-Mirédin, O.; Da Costa, G.; Blavette, D. Clustering and Nearest Neighbour Distances in Atom-Probe Tomography. *Ultramicroscopy* **2009**, *109* (10), 1304−1309.
(18) Rigutti, L.; Venturi, L.; Houard, J.; Normand, A.; Silaeva, E. P.; Borz, M.; Malykhin, S. A.; Obraztsov, A. N.; Vella, A. Optical Contactless Measurement of Electric Field-Induced Tensile Stress in Diamond Nanoscale Needles. *Nano Lett.* **2017**, *17* (12), 7401−7409.
(19) Birner, S.; Zibold, T.; Andlauer, T.; Kubis, T.; Sabathil, M.; Trellakis, A.; Vogl, P. Nextnano: General Purpose 3-D Simulations. *IEEE Trans. Electron Devices* **2007**, *54* (9), 2137−2142.
(20) Mancini, L.; Moyon, F.; Hernàndez-Maldonado, D.; Blum, I.; Houard, J.; Lefebvre, W.; Vurpillot, F.; Das, A.; Monroy, E.; Rigutti, L. Carrier Localization in GaN/AlN Quantum Dots As Revealed by Three-Dimensional Multimicroscopy. *Nano Lett.* **2017**, *17* (7), 4261−4269.
(21) Di Russo, E.; Mancini, L.; Moyon, F.; Moldovan, S.; Houard, J.; Julien, F. H.; Tchernycheva, M.; Chauveau, J. M.; Hugues, M.; Da Costa, G.; Blum, I.; Lefebvre, W.; Blavette, D.; Rigutti, L. Three-Dimensional Atomic-Scale Investigation of ZnO-MgxZn1-xO m-Plane Heterostructures. *Appl. Phys. Lett.* **2017**, *111* (3), 032108.
(22) Silaeva, E. P.; Arnoldi, L.; Karahka, M. L.; Deconihout, B.; Menand, A.; Kreuzer, H. J.; Vella, A. Do Dielectric Nanostructures Turn Metallic in High-Electric Dc Fields? *Nano Lett.* **2014**, *14* (11), 6066−6072.
(23) Chauveau, J.-M.; Laügt, M.; Venneguès, P.; Teisseire, M.; Lo, B.; Deparis, C.; Morhain, C.; Vinter, B. Non-Polara-Plane ZnMgO1/ZnO Quantum Wells Grown by Molecular Beam Epitaxy. *Semicond. Sci. Technol.* **2008**, *23* (3), 035005.
(24) Blum, I.; Cuvilly, F.; Lefebvre-Ulrikson, W. Atom Probe Sample Preparation. In *Atom Probe Tomography*; Academic Press, 2016; Chapter 4, pp 97−121, DOI: 10.1016/B978-0-12-804647-0.00004-8.

https://dx.doi.org/10.1021/acs.nanolett.0c03584
Nano Lett. XXXX, XXX, XXX−XXX